X-Ray Diffraction of Solid Tin to 1.2 TPa

A. Lazicki, J. R. Rygg, F. Coppari, R. Smith, D. Fratanduono, R. G. Kraus, G. W. Collins, R. Briggs, D. G. Braun, D. C. Swift, and J. H. Eggert

Phys. Rev. Lett. **115**, 075502 — Published 12 August 2015

DOI: 10.1103/PhysRevLett.115.075502

X-ray diffraction of solid tin to 1.2 TPa

A. Lazicki,[1] J. R. Rygg,[1] F. Coppari,[1] R. Smith,[1] D. Fratanduono,[1] R. G. Kraus,[1]
G. W. Collins,[1] R. Briggs,[2] D. G. Braun,[1] D. C. Swift,[1] and J. H. Eggert[1]

[1] *Lawrence Livermore National Laboratory, 7000 East Ave., Livermore, California 94550*
[2] *The University of Edinburgh, Mayfield Rd., Edinburgh, EH9 3JZ, United Kingdom*

We report direct *in situ* measurements of the crystal structure of tin between 0.12 and 1.2 terapascals, the highest stress at which a crystal structure has ever been observed. Using angle-dispersive powder x-ray diffraction, we find that dynamically-compressed Sn transforms to the body-centered-cubic (bcc) structure previously identified by ambient-temperature quasistatic-compression studies and by zero-kelvin density functional theory predictions between 0.06 and 0.16 TPa. However, we observe no evidence for the hexagonal close-packed (hcp) phase found by those studies to be stable above 0.16 TPa. Instead, our results are consistent with bcc up to 1.2 TPa. We conjecture that at high temperature bcc is stabilized relative to hcp due to differences in vibrational free energy.

The interplay between the electronic and vibrational contributions to the free energy of a crystal can lead to a rich and complex pressure-temperature phase diagram, especially interesting in regimes where a solid is compressed and heated to the extent that valence electrons are delocalized and standard chemical models for bonding break down. Sn is a particularly fascinating system to explore because the energetic advantage of sp^3 bonding (which gives the lighter group IV elements their tetrahedral structures), and the energy cost of promoting s-electrons to the p-band (which drives heavier Pb to take on a face-centered cubic structure) are nearly balanced. As a result Sn has several phases which are very close in energy and their relative stabilities are affected by differences in vibrational and electronic free energy contributions to the Gibbs free energy at finite temperature. The effects of temperature on phase stability, especially at extreme compression, are not often addressed experimentally or theoretically because of the difficulty of performing these studies (in spite of the fact that in the universe high pressure is almost always accompanied by temperatures higher than 300K). Dynamic compression is currently the only experimental method for reaching TPa stress states (1 TPa = 10 million atmospheres) and elevated temperatures simultaneously. In traditional shock wave experiments however, the discontinuous rise in entropy results in high temperature melted states long before TPa pressures are reached. Shocked Sn reaches the solidus of the melt transition at ∼0.05 TPa, precluding a study of its solid phases in the TPa regime. In this work we use laser ramp or multi-shock compression (nanosecond-scale rise-time) to probe TPa states below the melting temperature.

The solid phase diagram of Sn has been explored using static compression methods up to 0.2 TPa at 300K [1], and to 0.1 TPa up to the melting line [2]. In the ground state Sn takes on the α (diamond) structure [3], but transforms to the β (tetragonal; β-Sn) structure at 286 K [4]. With increasing pressure, Sn undergoes several more phase transitions: $\beta \rightarrow$ bct (body-centered-tetragonal) $\rightarrow$ bct/bco (body-centered-orthorhombic) mixed phase $\rightarrow$ bcc (body-centered-cubic) $\rightarrow$ hcp (hexagonal-close-packed) [1, 5, 6]. Theory predicts that, at 0 K, the hcp phase will persist up to ∼1.3 TPa, after which the bcc phase will again be stabilized [1]. However at 300 K and 0.22 TPa, the vibrational free energy of the bcc phase is predicted to be slightly lower than that of hcp [7], suggesting that high temperature may also stabilize the bcc phase relative to hcp.

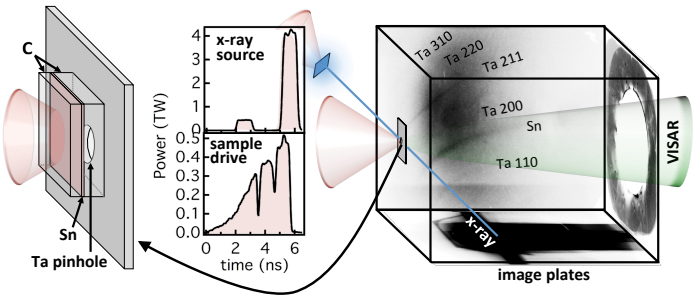

FIG. 1. Targets consist of ∼4 μm Sn foil between single crystal diamond plates of ∼20 μm (pusher) and ∼40 μm (tamper), joined by 1-2 μm layers of epoxy. In some targets, the pusher is formed from two ∼15-μm diamond plates sandwiching a 1-2 μm Au pre-heat shield.The target is backed by a 300 μm-diameter Ta or Pt pinhole which collimates scattered x-rays. The package is mounted on a box lined with image plates. He_α x-ray radiation from a laser-ablated metal foil (incident at 45°) is diffracted off the target and the Debye-Scherrer rings register as conic sections on the image plates.

We have succeeded in compressing solid Sn from 0.12 to nearly 1.2 TPa (the highest stress state diffraction measurements yet made) and conclude that the bcc phase is stable over this entire range, including the regime where lower-temperature static measurements find a hcp phase.

The experimental configuration is shown in Figure 1. Compression is accomplished by ablating a single-crystal ⟨110⟩ or ⟨100⟩-oriented diamond pusher with a temporally shaped laser pulse, creating a rapidly expanding high-energy plasma and generating a compression wave

that propagates into the diamond. An 800 μm laser spot size with a supergaussian profile is accomplished using distributed phase plates. The laser intensity is ramped up from 0 to a peak of $0.5 \rightarrow 20 \times 10^{13}$W/cm^2 over 3-4 ns, and maintained for 1-3 more nanoseconds with the goal of holding a steady stress state in the sample for at least 1 ns. Due to pulse-length limitations and target material response, the Sn drive is likely a multi-shock rather than a ramp in some of these experiments (Fig. S1). The compression wave traverses the diamond package, reverberating in the thin Sn and accelerating the rear diamond. The velocity history of the diamond free surface is measured using velocity interferometry (VISAR) [8, 9]. Details about the extraction of Sn stress from this velocity history are given in Ref. [10] and Figure S2. For highest-intensity drives (>700 GPa), a Au preheat shield between the sample and the ablated diamond is used to prevent preheating and melting of the Sn. At peak compression, x-ray radiation is generated by inducing He$_\alpha$ emission from a 13-μm foil (Fe or Cu) using a 1-ns duration laser pulse (with low-power prepulse to optimize x-ray conversion efficiency [11]). Lasers are defocused to a 300 μm spot without phase plates (peak irradiance on the order of 10^{15}W/cm^2).

Figure 2 shows sample diffraction data at selected stress states over the range in the study, with image plates digitally projected to display constant contours of Bragg angle 2θ, illustrating some of the typical features of these measurements. A spatially broad and smoothly varying background originating from x-rays created in the ablation plasma is subtracted from the images using a nonlinear peak clipping algorithm[12, 13]. Some spurious features on the image plates originate from materials positioned in the diagnostic box to absorb x-rays from the ablation plasma (such as the strips of plastic evident in Figure 2(a)) and from the He-β emission (such as the unintentionally wrinkled Cu metal foil evident in Figure 2(c)). In rare cases, scattering from another material in the target assembly or diagnostic box is registered on the image plate, as in Figure 2(b) near $2\theta \sim 93°$. The curvature of this feature indicates that its physical origin is not within the driven sample, and has therefore been masked out of the lineout shown in Figure 2(e). Scattering from the single crystal diamond windows is sometimes evident: at $2\theta \sim 87°$ in Figures 2(b) and 2(d) and at $\sim 45°$ in Figures 2(b-d). The peak is masked out in 2(d) because it is so intense that the image processing algorithm produces extended artifacts which obscure nearby data (see Figure S3(b) for the unmasked image). The position and character of these peaks are consistent with 111 and 311 reflections from diamond at <80 GPa (further details in Figure S3). The strong, continuous diffraction peaks marked with grey lines in Figures 2(a-d) are from the ambient-pressure pinhole material (platinum in Figure 2(a) and tantalum in Figures 2(b-d)), which are used for angular calibration of the image plates.

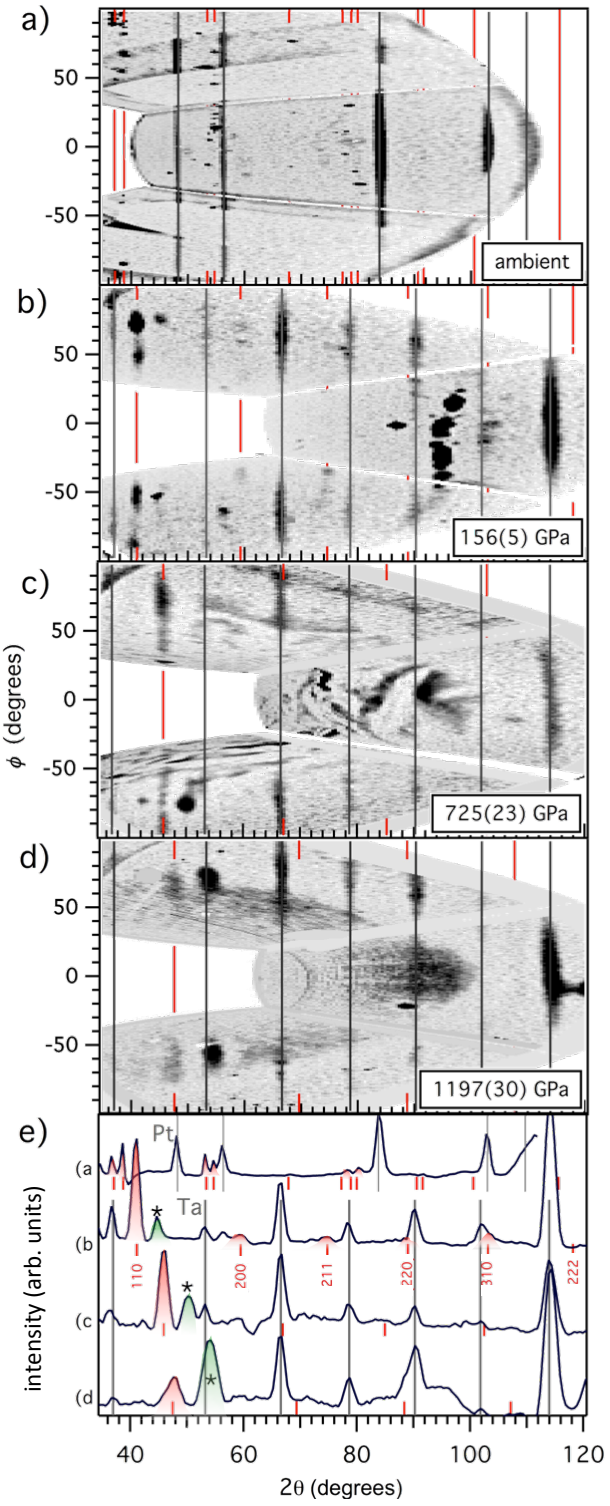

FIG. 2. X-ray diffraction measurements: a) Omega EP 13742, b) Omega 58709, c) Omega 66028, d) Omega 68278. Rectangular image plates are digitally warped to map from detector planes to azimuthal angle vs. Bragg angle. Ideal peak positions for the reference material used for image plate calibration are shown in grey, and Sn ideal peak positions assuming a tetragonal (a) and bcc (b-c) structure are shown with the red line segments. Suspected diamond peaks are labeled with an asterisk on the image plate lineouts shown in (e).

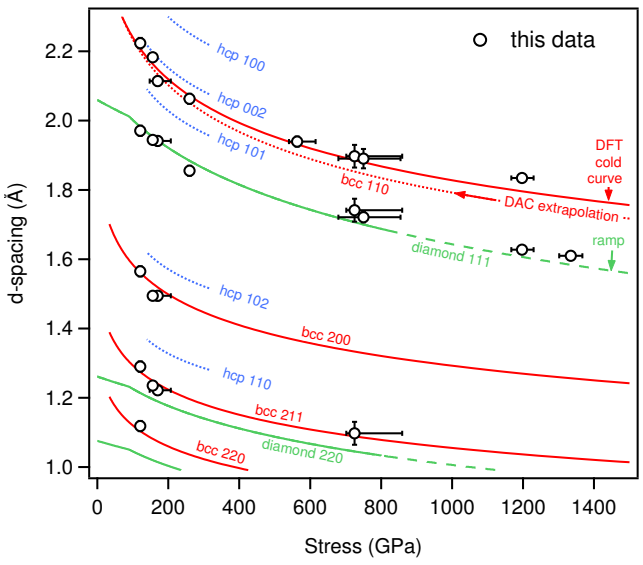

FIG. 3. d-spacing of observed diffraction peaks (data in Table S1), compared with the DFT cold curve (red solid line) [1] and with the isothermal equation of state trends and phase transition known from static experiments (dotted lines) [1, 5], extrapolated above 180 GPa. The green lines represent the expected trend in diamond d-spacing [17] (dashed line: extrapolation above 800 GPa)

Diffraction from ambient Sn (99.9% purity Goodfellow rolled foil) shown in Figure 2(a) is sparse and spotty, indicating that the foils have large, randomly-distributed crystallites. The ambient Sn data is consistent with the expected β-Sn structure, although there is some (<1%) deviation from ideal peak position, due to poor statistical sampling of large, mildly-strained crystallites.

From 120-170 GPa (Fig. 2(b)) Sn is in the bcc phase, consistent with the static compression measurements of the bcc phase up to at least 180 GPa [1]. The phase transition to bcc caused a significant change in the microstructure compared to the ambient scattering. The intensity variation as a function of azimuthal angle indicates preferred orientation of crystallites, but the distribution in ϕ and the smoothness of the peaks indicates decreased grain sizes. The stress-induced shifts in the peak positions agree well with the ideal shifts in d-spacing with stress for all peaks (Fig. 3, Table S1), indicating that the cubic crystal structure is not significantly distorted under the strong uniaxial loading.

Above 200 GPa, we observe only 1-3 diffraction peaks and their positions are not consistent with the transition to hcp observed in static measurements (Fig. 3). While this number of peaks is insufficient to uniquely identify a crystal structure, we narrow the range of possibilities by considering the density that the peak positions imply (density drops or large density jumps upon stress increase are considered unlikely) and the probability of observing the registered peak, based on the expected peak intensities for the hypothesized crystal symmetry. If we assume that there must be a transition to an hcp structure near 200 GPa (a martensitic transition and therefore likely to take place at these time scales [14]) and assign our two dominant peaks as the hcp 100 and 101 reflections, we find an unreasonably large density jump of ~11% (Fig. S4). An assignment of the higher d-spacing peak as the 002 peak from the hcp phase produces a smoother density trend, but is unlikely, based on the expectation that the 100 and 101 peak intensities should be greater for hcp symmetry. Unusual peak intensity ratios could occur if there is strong preferred orientation in the sample as a result of anisotropic response, but the 002 peak should not, in that case, be the most intense for this geometry [15]. The hexagonal ω phase, although not predicted to be stable for Sn, is another martensitic transition commonly observed in close-packed metallic systems [16], but a treatment of the two intense peaks as the 110 and 101 ω reflections would also require a 11-12% density jump.

The position and shift of the higher d-spacing peak is consistent with an extrapolation of the Sn bcc 110 peak shift [1], and the lower d-spacing peak is consistent with the expected diamond peak shift [17]. This latter peak (labeled with an asterisk in Figure 2(e)) is azimiuthally localized but more extended than the single-crystal diamond reflections, suggesting that the single crystals fragment upon compression and the crystallites adopt a distinct preferred orientation. This unusual behavior has not been positively verified, and further studies to understand the nature of single crystal diamond at extreme dynamic compression are underway. Based on the peak positions, however, we conclude that the most reasonable interpretation of these results is that Sn remains in the bcc phase; we do not see the hcp phase transition observed in static measurements; and the textured diffraction feature at lower d-spacing originates from diamond. Given the lack of texture and the relatively high signal-to-background (~0.45) of the Sn peak, and assuming the structure is indeed bcc, several higher angle peaks would be expected to be observable above the background. This lack of intensity in the higher angle peaks suggests a large mean-square displacement and a small Debye-Waller factor, consistent with temperatures in the thousands of Kelvin. However, a reliable evaluation of the Debye-Waller factor to estimate temperature requires an accurate account of lattice anharmonicity and volume dependence of the Debye temperature, which is beyond the scope of this paper.

Above 1 TPa, the Sn peak has broadened and weakened compared to lower-stress measurements, possibly indicating more significant heating or closer proximity to melt, since it can be correlated with the formation of a strong shock in the velocity history at the rear diamond surface of the target (Fig. S3(b)). Because dynamically compressed diamond loses transparency beyond the elastic limit due to fracture, it is impossible to determine

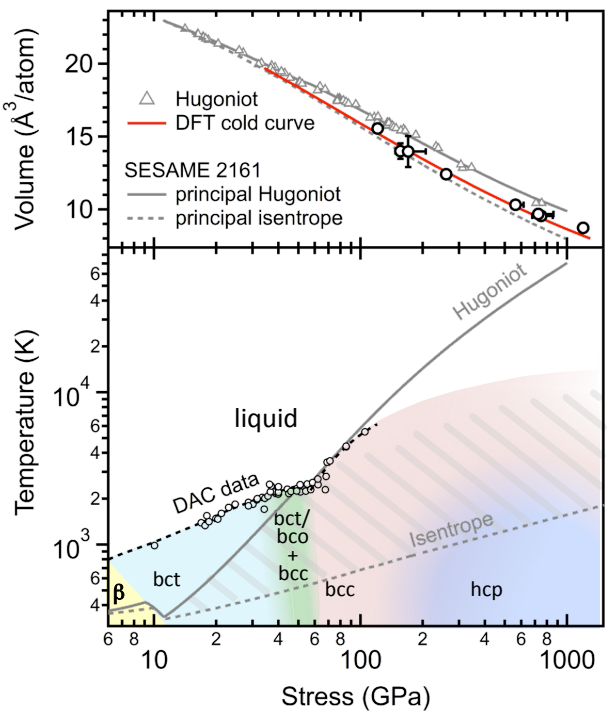

FIG. 4. Top: equation of state of Sn, assuming a bcc phase, compared to the DFT cold curve [1], Hugoniot data [21] and tabulated EOS model SESAME 2161 [18]. Bottom: Phase diagram of Sn known from static and shock studies [1, 2, 22–24]. The thermodynamic path followed in this study is unknown but the temperature is bounded by the grey hashed region.

precisely where the shock formed within the sample, but it is possible that Sn is more strongly heated. One shot at 1.33 TPa which also displayed a strong shock at the diamond free surface had no distinguishable diffraction from Sn (Fig. S3), suggesting that at these conditions the sample may have melted entirely.

The experimental equation of state of Sn is shown in Figure 4, assuming that the bcc structure is maintained over the entire stress range. The compressibility falls between the SESAME 2161 principal isentrope and Hugoniot [18]. The lower panel of Figure 4 illustrates the current understanding of the Sn phase diagram, and the region of phase space which our results inform. All previous measurements and theoretical predictions of the hcp phase have been made between 0-300K. The thermodynamic path for ramp-compressed materials is bounded at lower temperature by the principle isentrope and at upper temperature by the second-shock Hugoniot from an initial shock to ∼70 GPa (which represents the strength of the diamond elastic shock transmitted into Sn [19]). Accurate methods for measuring temperature remain an important challenge. Temperature estimates for a multi-shock path based on EXAFS measurements have been made for iron [20], showing that the temperature falls roughly midway between the isentrope and the Hugoniot.

There are at least two possible explanations for the different dynamic- and static-compression phase observations: the hcp phase may not be the energetically stable phase at the high temperatures in our experiment, or the strain rates in our experiment may be too rapid for nucleation and growth of the hcp phase to be observed. The activation free energy barrier to formation of the hcp phase in the Sn system (and the effect of pressure on that barrier) has not been reported so we cannot rule out the possibility of a kinetically hindered transition. However, metadynamics simulations at 200 GPa and 300K find that the transition is initiated in the very first timestep, indicating a very low free-energy barrier to formation of hcp [7].

The presence of a high-temperature bcc phase stabilized over hcp (or similarly close-packed fcc) is in fact common for elemental metals across the periodic table (including electronically similar Pb [25]) and the mechanism extensively discussed [26–30]. The bcc structures generally have softer phonons (slightly lower Debye temperature) than the close-packed phases, giving them higher vibrational entropy. They also tend to have a higher density of electronic states at the Fermi level, and thus higher electronic entropy. The higher total entropy in the bcc phase will diminish the free energy difference between the two phases at high temperature[31, 32]. When anharmonicity is taken into account the stability of bcc relative to hcp is even higher. In many cases when hcp is the stable ground state phase and bcc is observed experimentally at high temperature, theoretical calculations significantly overestimate the transition temperature unless the anharmonicity is accurately modeled. This demonstrates that anharmonic phonon contributions to the free energy at high temperature play an important role in counter-balancing the lower enthalpy of the hcp phase [30].

The ground state free energy difference between the bcc and hcp phases in Sn is very small (<40 meV/atom over the entire pressure range where hcp is stable [1, 7]). Even within the harmonic approximation, by 300 K the vibrational free energy of bcc is already predicted to be slightly lower than that of hcp [7]. It is likely that, should anharmonic affects be taken into account and first-principles calculations extended to thousands of Kelvin, bcc will be stabilized relative to hcp for Sn.

To summarize, we have performed x-ray diffraction measurements from 0.12 to 1.2 TPa, which is the highest stress state at which crystal structure has ever been directly probed. Our results suggest that the bcc phase is stable over this entire range, in contrast to quasistatic loading experiments at room temperature which find an hcp phase. Kinetic effects may play a role in supressing the transition to hcp, but it is also plausible that bcc is stabilized below the melting curve by differences in vibrational free energy which could compensate for the

lower ground state enthalpy of the hcp phase. These results demonstrate that temperature can play a significant role in stabilizing unpredicted phases at extreme conditions, and emphasize the importance of considering finite temperatures in structure prediction, and for developing methods for accurately measuring temperature.

We acknowledge: helpful discussions with P. F. McMillan, D. Klug, Y. Yao, L. Burakovsky, A. Salamat and C. Pickard; target fabrication by S. Uhlich, W. Unites and T. Uphaus; and support at the Laboratory for Laser Energetics by C. Sorce, N. Whiting and J. Tellinghuisen. This work was performed under the auspices of the U.S. Department of Energy by Lawrence Livermore National Laboratory under Contract DE-AC52-07NA27344. Lawrence Livermore National Security, LLC

[1] A. Salamat et al., Phys. Rev. B **84**, 140104(R) (2011).
[2] R. Briggs et al., J. Phys: Conf. Ser. **377**, 012035 (2012).
[3] A. Jayaraman, Rev. Mod. Phys. **55**, 65 (1983).
[4] J. D. Barnett, V. E. Dean, and H. T. Hall, J. Appl. Phys. **37**, 875 (1966).
[5] S. Desgreniers, Y. K. Vohra, and A. L. Ruoff, Phys. Rev. B **39**, 10359 (1989).
[6] A. Salamat et al., Phys. Rev. B **88**, 104104 (2013).
[7] Y. Yao and D. Klug, Solid State Comm. **151**, 1873 (2011).
[8] L. M. Barker and R.E. Hollenbach, J.Appl.Phys. **43**, 4669 (1972).
[9] P. M. Celliers et al., Rev. Sci. Instrum. **75**, 4916 (2004).
[10] J. R. Rygg et al., Rev. Sci. Instrum. **83**, 113904 (2012).
[11] D. Babonneau et al., Phys. of Plasmas **15**, 092702 (2008).
[12] C. G. Ryan et al., Nucl. Instr. and Meth. B **34**, 396 (1988).
[13] M. Morhac et al., Nucl. Instr. and Meth. A **401**, 113 (1997).
[14] N. V. Chandra Shekar and K. Govinda Rajan, Bull. Mater. Sci., **24**, 1 (2001).
[15] H.-R. Wenk et al., Nature **405**, 1044 (2000).
[16] S. K. Sikka, Y. K. Vohra and R. Chidambaram, Progress in Materials Science, **27**, 234 (1982).
[17] D. K. Bradley et al., Diamond at 800 GPa, Phys. Rev. Lett. **102**, 075503 (2009).
[18] C. Greeff et al., SESAME 2161: An explicit multiphase equation of state for tin, LA-UR-05-9414 (2005).
[19] R. S. McWilliams et al., Phys. Rev. B **81**, 014111 (2010).
[20] Y. Ping et al., Phys. Rev. Lett. **111**, 065501 (2013).
[21] Russian shock wave database (http://teos.ficp.ac.ru/rusbank/)
[22] B. Schwager et al., Chem. Phys. **133**, 084501 (2010).
[23] P. L. Hereil and C. Mabire, J. Phys. IV France **10** Pr9 (2000)
[24] J. Hu et al., J. Appl. Phys. **104**, 083520 (2008).
[25] A. Dewaele et al., Phys. Rev. B **76**, 144106 (2007).
[26] S. Alexander and J. McTague, Phys. Rev. B **41**, 702 (1978).
[27] J. Friedel, J. Phys. Lett. (Paris) **35**, 159 (1974).
[28] R. E. Watson and M. Weinert, Phys. Rev. B **30**, 1641 (1984).
[29] G. Grimvall et al., Reviews of Modern Physics **84**, 945 (2012).
[30] P. Souvatzis et al., Phys. Rev. Lett. **100**, 095901 (2008).
[31] E. G. Moroni, G. Grimvall and T. Jarlborg, Phys. Rev. Lett. **76**, 2758 (1996).
[32] S. R. Nishitani, H. Kawabe and M. Aoki, Materials Science and Engineering: A **312**, 77 (2001).
[33] See Supplemental Material [url], which includes Refs. [34–37]
[34] D. E. Fratanduono et al., J. Appl. Phys. **110**, 073110 (2011).
[35] S. Brygoo et al., Nature Materials **6**, 274 (2007).
[36] J. H. Eggert et al., Nature Physics **6**, 40 (2010).
[37] M. D. Knudson et al., Science **322**, 1822 (2008).